

# Hybridizing ZnO Nanowires with Micropyramid Silicon Wafers as Superhydrophobic High-Efficiency Solar Cells

Yan Liu, Arnab Das, Sheng Xu, Ziyin Lin, Chen Xu, Zhong Lin Wang, Ajeet Rohatgi, and Ching Ping Wong\*

Low conversion efficiency is still the main limiting factor for current solar-cell technologies. A large portion of the energy loss during solar-cell operation is attributed to optical loss, namely the loss of the incoming light by reflection.<sup>[1]</sup> To reduce the reflection loss, surface texturing and antireflection coatings are the most-commonly used strategies.<sup>[2–4]</sup> Surface texturing is able to enhance light trapping by multiplying the internal reflections. The industrial standard for the current Si-based photovoltaic (PV) industry process is alkaline fabrication of micrometer-sized pyramid textures. An emerging focus today is the incorporation of nanostructures as surface-texturing materials.<sup>[5–8]</sup> For example, porous Si and Si nanowires (NWs) have been applied to solar cells to effectively reduce the reflection loss.<sup>[9–11]</sup> Xiu et al. developed a hierarchical structure through a two-tier texturing method for lower light reflection.<sup>[12]</sup> Using an antireflection coating (ARC) is another method to reduce light reflectance via destructive interference of the reflected light at the air–ARC–substrate interfaces. A single-layer ARC, such as silicon nitride (SiN<sub>x</sub>), is the industry standard ARC on Si PVs.<sup>[13]</sup> A further reduction of reflection can be achieved through a multilayer ARC or fine control of the ARC geometry, which enables a gradual transition of the refraction index from air to the silicon.<sup>[14,15]</sup>

As an outstanding 1D nanostructure, ZnO NWs have a high transparency due to the wide bandgap, appropriate refractive index ( $n \approx 2$  at 600 nm), and the capability of forming a textured coating on virtually any substrate.<sup>[16–19]</sup> These characteristics make it an attractive dielectric ARC material for PV applications. By the integration of ZnO NWs with optical fibers and quartz waveguides, an enhancement of the efficiency by a factor of 4–6 has been shown by utilizing a three-dimensional approach.<sup>[20,21]</sup> The application of ZnO nanostructures on planar Si as an ARC for solar cells has achieved a weighted reflectance

(WR) of 6.6%<sup>[22]</sup> and a conversion efficiency of 12.8%.<sup>[23]</sup> Since high-efficiency cells are typically textured to take advantage of their light-scattering/trapping effect, a further boost to the solar-cell efficiency is expected by introducing a ZnO-NW-based hierarchical nanostructure.

In this study, we report a novel hierarchical structure, integrating ZnO-NW arrays on Si micropyramids, as an effective ARC for improving the energy-conversion efficiency. In the past, the ability to use industrial contacting techniques and the physical robustness of the NWs have not been demonstrated. As the screen-printing of metal electrodes is the dominant contact method for silicon solar cells, this work examines the ability to contact solar cells through an NW ARC layer. In addition, the ARC layers must be abrasion resistant to survive the screen-printing process and be useful over the 25-year lifespan of a typical cell module. We have therefore also examined the effect of abrasion on the hierarchical nanostructure during screen-printing, the ARC effect and the nonwetting of such a structure. The ZnO NWs on the Si micropyramids allow a gradual transition of the effective refractive index from air to the Si, while the pyramidal-Si surface multiplies light reflections within the hierarchical structure. As a result, this structure displays a broadband reflection suppression in the 300–1200 nm range, with an average weighted reflectance of 3.2%. A conversion efficiency of 16.0% was obtained, which is the highest for any solar cell fabricated using ZnO nanostructures as the ARC layer. In addition, surface modification enables a superhydrophobicity that prevents the blocking of light by dust particles on solar panels.

The structure of the solar cell, with ZnO NWs on Si pyramids, is schematically shown in **Figure 1**. The Si substrate used was a single-crystal, p-type float-zone substrate with a thickness of 300  $\mu\text{m}$ . The textured Si surface with pyramidal structures was created by KOH etching. The wafers were then cleaned to remove surface organic and metallic contaminants, followed by POCl<sub>3</sub> diffusion to form the n<sup>+</sup>-emitter. A diffusion temperature of 860 °C was used to obtain a 65  $\Omega$  per sq emitter. After the removal of phosphorus-glass in a buffered HF solution, a SiO<sub>2</sub> passivation layer was grown at 900 °C. The treated wafer was used for ZnO-NW growth by a low-cost and scalable hydrothermal method.<sup>[24]</sup>

After the growth of the ZnO NWs, screen-printed n<sup>+</sup>-p-p<sup>+</sup> solar cells (4 cm<sup>2</sup>) were fabricated. The surface morphology of the ZnO NWs on the Si pyramids is shown in **Figure 2**. The size of the Si micropyramids was around 2–4  $\mu\text{m}$  (**Figure 2a**). Highly dense ZnO NWs were hierarchically grown on top of the micropyramids (**Figure 2b**). Most of the ZnO NWs were perpendicular to the Si pyramids, due to their anisotropic growth along the *c*-axis. The morphology of ZnO-NW arrays

Y. Liu, S. Xu, Z. Lin, C. Xu, Prof. Z. L. Wang, Prof. C. P. Wong  
School of Materials Science and Engineering  
Georgia Institute of Technology  
Atlanta, GA 30332-0245, USA  
E-mail: cp.wong@mse.gatech.edu

A. Das, Prof. A. Rohatgi  
School of Electrical and Computer Engineering  
Georgia Institute of Technology  
Atlanta, GA 30332-0250, USA

Prof. C. P. Wong  
Faculty of Engineering  
The Chinese University of Hong Kong  
Shatin, NT, Hong Kong

DOI: 10.1002/aenm.201100287

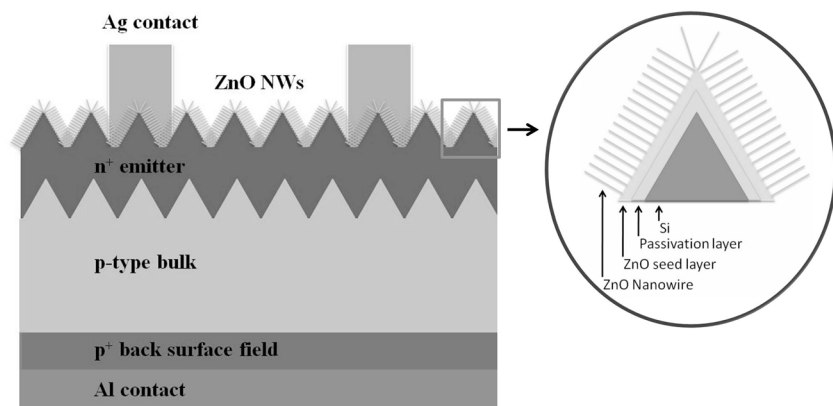


Figure 1. A schematic of the hierarchical ZnO NW-Si solar cell.

can be controlled by modifying the seed-layer thickness and the corresponding growth parameters.<sup>[25]</sup> The length of the ZnO NWs was measured from the cross-section view. As seen from Figure 2c, the ZnO NWs had a length of  $\approx 800$  nm. This length was chosen according to a ray-tracing-simulation optimization, which will be discussed later.

The average weighted reflectance (AWR) was calculated from the hemispherical reflectance spectrum (300–1200 nm) measured in our study. Figure 3a compares the measured front reflectance of the bare planar-Si surface and the Si-pyramid surface with and without ZnO NWs on top. The bare planar-Si surface reflected  $\approx 34.8\%$  of incident sunlight. The textured pyramid surface improved light trapping by doubling the bounces of the incident light, and reduced the light reflection to 11.3%. The deposition of the ZnO seed layer on the Si micropylramids as an ARC resulted in a significant reduction of light reflection in all of the UV, visible-light and IR regions, with an AWR of 4.1%. After applying the ZnO NWs on the seed layer, a further suppression of light reflectance was observed. An AWR suppression as low as 3.2% was achieved with the ZnO-NW hierarchical structure, which is much lower than the previously reported 6.6% AWR of tapered ZnO nanostructures grown on planar-Si surfaces.<sup>[22]</sup> An effective refractive index can be calculated by averaging the refractive indices of air and ZnO, weighted by the volume at the interface between the air and the ZnO, as pointed out by Zhu et al.<sup>[26]</sup> The enhanced WR suppression of the hierarchal structure is attributed to the effect of microscale texturing, which allows two bounces of light at the surface and a more-gradually changing effective refractive index from air to the Si substrate, compared with a single ZnO-seed-layer ARC (Figure S1, Supporting Information).

A better understanding of the effect of the hierarchical structure on the reflectance suppression was obtained by a Monte Carlo ray-tracing simulation using the Sunrays 1.3 program. The reflectance spectra of our textured solar cells were analyzed by varying the parameters of the ZnO-NW ARC. The simulation takes into account the 3D surface geometry of the simulated structure, as well as the optical properties (surface roughness, index of refraction and extinction coefficient) of every layer and interface, in order to quantify the reflection and absorption in the structure.<sup>[27]</sup> We employed a 300  $\mu\text{m}$ -thick Si layer with an upright-pyramid front texture in the simulation. The surface

coating on the Si pyramids was divided into three layers: a bottom passivation layer of  $\text{SiO}_2$  (15 nm), a middle ZnO seed layer (variable thickness) and a top ZnO-NW layer (variable thickness). The dispersion relation ( $n$  and  $k$ ) for crystalline ZnO was obtained from the literature<sup>[28]</sup> and provided as an input to Sunrays (shown in Figure S2, Supporting Information). The ZnO NWs in our structure were estimated to be a volume fraction of  $\approx 70\%$  from the calculation of many scanning-electron-microscopy (SEM) cross sections, and the effective refractive index ( $n$ ) of the ZnO-NW layer was calculated as being the sum of 70%  $n_{\text{ZnO NW}}$  and 30%  $n_{\text{air}}$ .

Initial simulations showed strong interference fringes in the simulated reflectance

curves (Figure S4, Supporting Information), which is similar to that which has been reported using rigorous coupled-wave-analysis (RCWA) simulations.<sup>[22]</sup> The SEM cross-sectional image (Figure 2c) indicates that the length of most of the NWs varied by  $\pm 75$  nm from the average NW length ( $h$ ). Therefore, for each NW length that was simulated, three reflectance spectra ( $h$ ,  $h - 75$  nm and  $h + 75$  nm) were generated and averaged. The resulting reflectance spectrum showed an almost complete suppression of interference fringes (Figure S4, Supporting Information).

In order to optimize the light reflection of the ZnO-NW solar cell, we modified the ZnO-NW parameters in Sunrays 1.3, including the thickness of the seed layer and the length of the ZnO NWs (Figure S3, Supporting Information). The simulation results are listed in Table S1, Supporting Information and Table S2, Supporting Information. When optimizing the thickness of the seed layer in the 20–100 nm range, with a constant ZnO-NW length of 800 nm, the weighted reflectance had a minimum of 3.3% for a seed-layer thickness of 60 nm. For the NW-length optimization in the 200–1500 nm range with a constant seed-layer thickness of 60 nm, the same minimal value of 3.3% was obtained for an NW length of 800 nm. Under air mass (AM) 1.5, it is desirable to fully utilize the visible-light region while still maintaining low reflection in the UV and IR regions. Therefore, an NW length of  $\approx 800$  nm with a seed layer of 60 nm was chosen, and the resulting reflectance curve with an AWR of 3.3% matched very well with the experimental reflectance spectra (Figure 3b). Sunrays 1.3 also calculates the short-circuit current  $J_{\text{sc}}$  under the AM1.5 spectrum, assuming a 100% internal quantum efficiency (IQE). For pyramidal solar cells with a thin  $\text{SiO}_2$  passivation layer only (no ARC layer),  $J_{\text{sc}}$  was 38.18  $\text{mA cm}^{-2}$ . The additional 60 nm ZnO seed layer resulted in a  $J_{\text{sc}}$  of 38.78  $\text{mA cm}^{-2}$ , and the ZnO-NW ARC layer (60 nm ZnO seed layer and 800 nm ZnO NWs) on top of the  $\text{SiO}_2$  layer resulted in a  $J_{\text{sc}}$  of 40.86  $\text{mA cm}^{-2}$ , which is a 7.0% enhancement over the case with the  $\text{SiO}_2$  layer only. In addition, the Sunrays 1.3 simulation showed that ZnO NWs on a textured surface enable a significantly lower light reflectance than ZnO NWs on planar surfaces with the same ZnO-NW dimensions (length and thickness of seed layer, Figure 3b). This further confirms the effect of Si surface texturing in reflection suppression, as we discussed before.

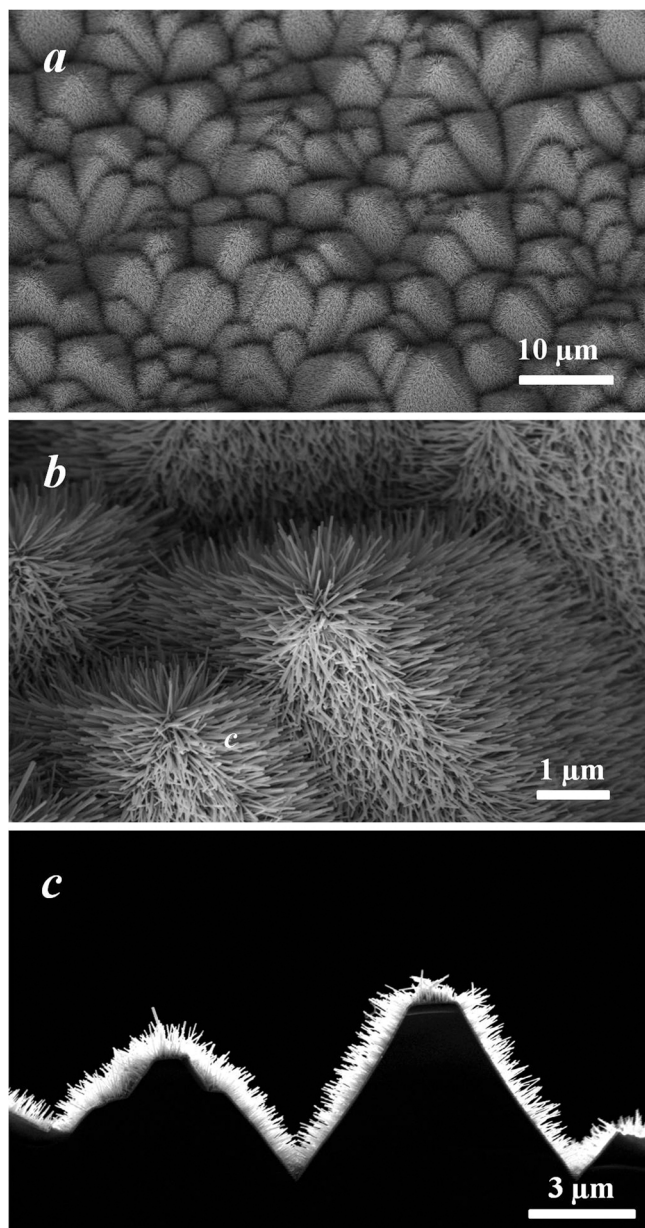


**Figure 2.** a,b) Surface morphology of the hierarchical ZnO NWs on the pyramidal Si surfaces under low (a) and high (b) magnifications. c) Cross-sectional view of the hierarchical ZnO NWs on the pyramidal Si surfaces.

To prove the applicability of the ZnO NWs as an ARC for industrially processed Si solar cells, we fabricated screen-printed-aluminum back-surface-field (Al-BSF) solar cells with the optimized ZnO-NW parameters. The Al-BSF provided the back-surface passivation.<sup>[29]</sup> The thermal stability and mechanical robustness of the ARC is an important characteristic, as the screen-printed cells must survive under the pressure of the printing process from the screen and the short contact-firing cycle at 700–800 °C. The difference in the AWR of the ZnO-NW ARC before and after screen-printing was smaller than 0.1%. For the screen printed n<sup>+</sup>-p-p<sup>+</sup> solar cell (Figure 1),

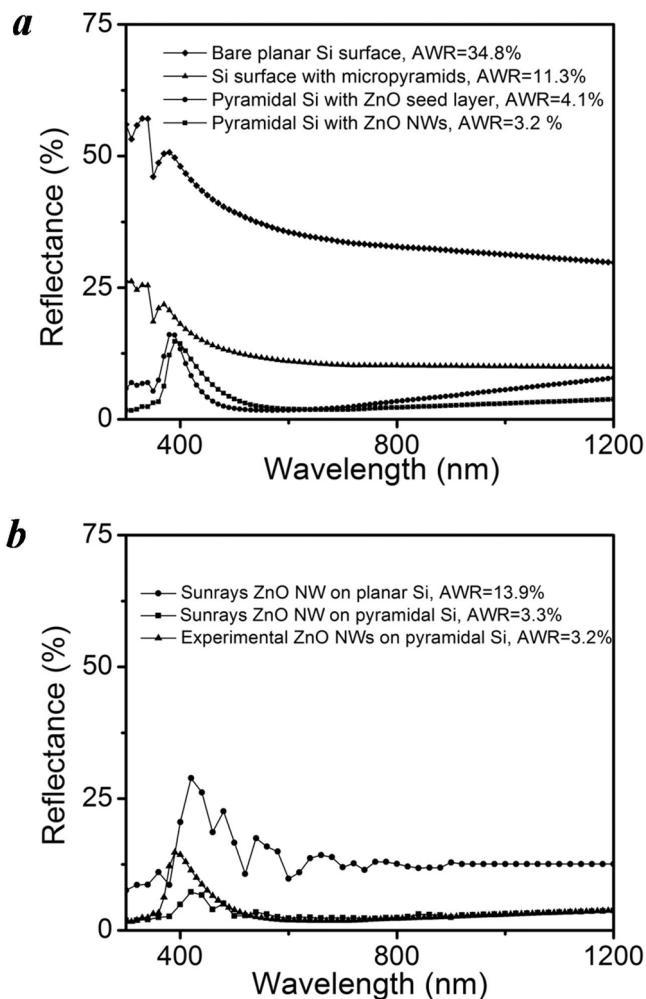


**Figure 3.** a) Front light reflectance of ZnO NWs on pyramidal Si, compared with planar Si, pyramidal Si and pyramidal Si with a ZnO seed layer. b) Simulated light reflectance of the ZnO-NW solar cell.

the ZnO NWs acted as an ARC layer, and the SiO<sub>2</sub> helped to improve the front-surface passivation. The advantages of using a ZnO-NW array with conventional cell structure are: 1) rapid application to an industrially proven solar-cell structure and 2) a mature platform that will facilitate further optimization and characterization of the reflection/light-trapping properties of NW arrays. The cell performance was characterized by the *I*-*V* curve under the condition of AM 1.5 illumination (Figure 4). The hierarchical ZnO-NW/pyramidal-Si solar cells exhibited a conversion efficiency of up to 16.0% with an open-circuit voltage of 616.3 mV, a short-circuit current of 35.3 mA cm<sup>-2</sup> and a fill factor of 73.4%. This is a very high efficiency for ZnO-nanostructure-decorated silicon-based solar cells and is comparable with commercial SiN<sub>x</sub>-coated solar cells. The cells fabricated in this work used commercial Ag pastes that were formulated to provide an ohmic contact to the n<sup>+</sup>-Si after etching through the industry-standard SiN<sub>x</sub> ARC – a process known as “fire through”. However, the ZnO NWs were found to be much more resistant to etching than SiN<sub>x</sub>, resulting in either: 1) little or no contact between the Ag and the Si, or 2) partial junction



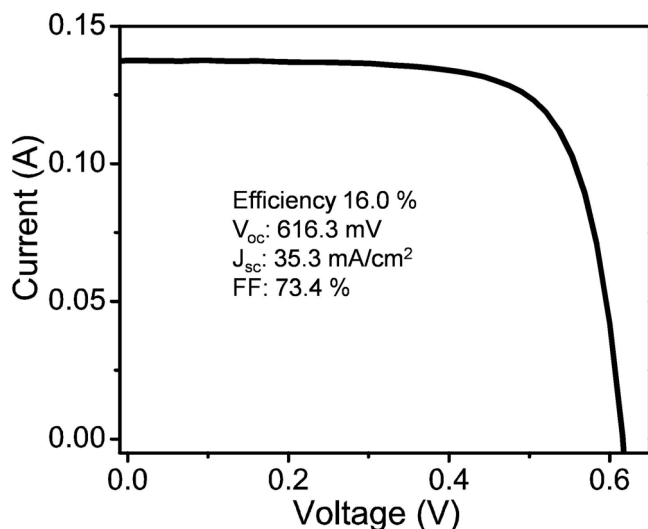


Figure 4. *I*-*V* curve of ZnO-NW/pyramidal-Si screen-printed solar cells.

shunting if the firing temperature was increased, increasing the etch rate and ensuring a complete etching of the NWs. The latter method provided the best contacts but was also responsible for the modest fill factors achieved on our best cells. Therefore, we believe that the efficiency of our solar cells can be further improved by increasing the fill factor through the use of an optimized Ag paste and firing conditions. In order to quantify the effect of the ZnO-NW ARC on the cell performance, we modeled the cell using the widely used solar-cell simulation program, PC1D,<sup>[30]</sup> and obtained a fit to both the IQE and the *I*-*V* data of the cell (Figure S5, Supporting Information and Table S3, Supporting Information). A lower conversion efficiency of 14.6% was obtained with an open-circuit voltage of 616.7 mV, a short-circuit current of 32.0 mA cm<sup>-2</sup> and a fill factor of 73.9%.

For solar cells, shading is an important practical issue for light absorption, because dust accumulation on the panel surface blocks the incident light and reduces the power output. In order to reduce dust accumulation on the solar-cell surface, a superhydrophobicity was applied to the solar cell by surface functionalization of the hierarchical structure. Superhydrophobic self-cleaning surfaces have shown water contact angles larger than 150° with hysteresis smaller than 10°.<sup>[31–34]</sup> To fabricate the superhydrophobic surface, a low surface energy and surface texturing are necessary. It is well-known that the surface free energies of the various crystallographic planes differ significantly. The wurtzite-structured ZnO grows fastest along the *c*-axis, and thus exposes the relatively low-energy side surfaces. The hierarchical structure presented in this study amplifies the hydrophobicity due to air trapped in between the individual NWs. Therefore, the initially prepared structure showed both a relatively low surface energy and a high surface roughness, with a high water-contact angle of 162.0 ± 2° and a contact-angle hysteresis of 18°. After hydrophobic coating with perfluoro-octyl trichlorosilane (PFOS) and a thermal treatment at 80 °C for 1 h, the surface energy was further reduced and a self-cleaning surface with a contact angle of 171.2 ± 1.8° and a hysteresis of

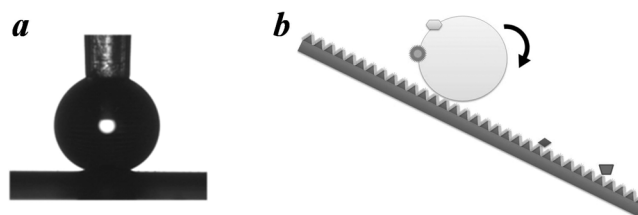


Figure 5. a,b) Superhydrophobic ZnO-NW solar cell: water droplet on self-cleaning surface with a contact angle of 171.2° (a); schematic view of the self-cleaning property (b).

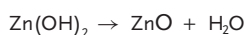
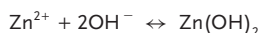
1.9° was obtained. For cells without a ZnO-NW antireflection coating, the contact angle of the surface was only 137.4 ± 0.9° after PFOS coating. As shown in Figure 5b, the superhydrophobic ZnO-NW-coated surfaces could effectively prevent dust accumulation on the solar-cell surface and this will help maintain the high-power-output performance of devices.<sup>[35]</sup>

In summary, we have demonstrated a superhydrophobic, high-efficiency solar cell based on ZnO NWs decorated on Si micropyramids as an antireflection coating. The ZnO NWs provide effective antireflection with a weighted reflectance of 3.2% over the 300–1200 nm spectral range. A screen-printed solar cell based on this hierarchical structure showed a high conversion efficiency of 16.0%. Moreover, the functionalized hierarchical surface enabled superhydrophobic and self-cleaning properties of the solar cell.

## Experimental Section

**Si Etching:** The textured Si wafer with micropyramids was created by KOH etching at 80–85 °C for 20–30 min. The etching solution was composed of KOH (2 wt%), water, and isopropyl alcohol (5 vol%).

**ZnO-Nanowire Growth:** A ZnO seed layer was deposited onto the SiO<sub>2</sub> layer by magnetron sputtering under an O<sub>2</sub> and Ar atmosphere (5 mTorr) without additional heating. The coated Si wafer was then placed in an aqueous solution containing hexamethylenetetramine (HMTA) and zinc nitrate hexahydrate. The reactions were performed at 80 °C as follows:



**Solar-Cell Fabrication:** Firstly, an Al paste was screen-printed on the reverse side of the Si substrate and dried at 200 °C. Ag grids were then screen-printed on top of the ZnO NWs, followed by co-firing of both the Ag and Al contacts. During the firing step, an Al-doped Si layer, referred to as the aluminum back surface field, was also formed. To prevent erroneous measurements, the active area of the cells was defined using a dicing saw, which electrically isolated each cell from the rest of the substrate.

**Solar-Cell Characterization:** The light reflectance was tested using a commercially available Optronic Laboratories OL 750 spectrophotometer with an integrating sphere at the University Center of Excellence for Photovoltaics Research and Education (UCEP) at the Georgia Institute of Technology. The details of the calibration are described in the supporting information. The solar-cell efficiency was measured using an *I*-*V* tester, which was calibrated using a calibration standard cell, measured at the

National Renewable Energy Laboratory (NREL). The calibration was performed before each measurement.

## Supporting Information

Supporting Information is available from the Wiley Online Library or from the author.

## Acknowledgements

The authors would like to acknowledge financial support from the National Science Foundation (NSF CMMI No. 0621115), and helpful discussions with Dr. Kyoung Sik Moon and Dr. Daniela Staiculescu.

Received: June 1, 2011  
Revised: October 3, 2011  
Published online:

- [1] A. J. Moule, K. Meerholz, *Appl. Phys. B - Lasers Opt.* **2007**, *86*, 721.  
[2] M. A. Green, *Adv. Mater.* **2001**, *13*, 1019.  
[3] W. L. Min, B. Jiang, P. Jiang, *Adv. Mater.* **2008**, *20*, 3914.  
[4] S. L. Diedenhofen, G. Vecchi, R. E. Algra, A. Hartsuiker, O. L. Muskens, G. Immink, E. Bakkers, W. L. Vos, J. G. Rivas, *Adv. Mater.* **2009**, *21*, 973.  
[5] Y. B. Tang, Z. H. Chen, H. S. Song, C. S. Lee, H. T. Cong, H. M. Cheng, W. J. Zhang, I. Bello, S. T. Lee, *Nano Lett.* **2008**, *8*, 4191.  
[6] Z. L. Wang, *Mater. Sci. Eng. R: Rep.* **2009**, *64*, 33.  
[7] W. U. Huynh, J. J. Dittmer, A. P. Alivisatos, *Science* **2002**, *295*, 2425.  
[8] Y. F. Huang, S. Chattopadhyay, Y. J. Jen, C. Y. Peng, T. A. Liu, Y. K. Hsu, C. L. Pan, H. C. Lo, C. H. Hsu, Y. H. Chang, C. S. Lee, K. H. Chen, L. C. Chen, *Nature Nanotechnol.* **2007**, *2*, 770.  
[9] H. B. Xu, N. Lu, D. P. Qi, J. Y. Hao, L. G. Gao, B. Zhang, L. F. Chi, *Small* **2008**, *4*, 1972.  
[10] K. Q. Peng, X. Wang, X. L. Wu, S. T. Lee, *Nano Lett.* **2009**, *9*, 3704.  
[11] P. Menna, G. Difrancia, V. Laferrara, *Sol. Energy Mater. Sol. Cells* **1995**, *37*, 13.  
[12] Y. H. Xiu, S. Zhang, V. Yelundur, A. Rohatgi, D. W. Hess, C. P. Wong, *Langmuir* **2008**, *24*, 10421.  
[13] J. Kim, J. Hong, S. H. Lee, *J. Korean Phys. Soc.* **2004**, *44*, 479.  
[14] X. Li, J. P. Gao, L. J. Xue, Y. C. Han, *Adv. Funct. Mater.* **2010**, *20*, 259.  
[15] S. Chhajed, M. F. Schubert, J. K. Kim, E. F. Schubert, *Appl. Phys. Lett.* **2008**, *93*.  
[16] Z. W. Pan, Z. R. Dai, Z. L. Wang, *Science* **2001**, *291*, 1947.  
[17] S. Xu, Y. Wei, M. Kirkham, J. Liu, W. Mai, D. Davidovic, R. L. Snyder, Z. L. Wang, *J. Am. Chem. Soc.* **2008**, *130*, 14958.  
[18] J. I. Hong, J. Bae, Z. L. Wang, R. L. Snyder, *Nanotechnology* **2009**, *20*, 085609.  
[19] M. Otto, M. Kroll, T. Käsebier, S. M. Lee, M. Putkonen, R. Salzer, P. T. Miclea, R. B. Wehrspohn, *Adv. Mater.* **2010**, *22*, 5035.  
[20] B. Weintraub, Y. G. Wei, Z. L. Wang, *Angew. Chem. Int. Ed.* **2009**, *48*, 8981.  
[21] Y. G. Wei, C. Xu, S. Xu, C. Li, W. Z. Wu, Z. L. Wang, *Nano Lett.* **2010**, *10*, 2092.  
[22] Y. J. Lee, D. S. Ruby, D. W. Peters, B. B. McKenzie, J. W. P. Hsu, *Nano Lett.* **2008**, *8*, 1501.  
[23] J. Y. Chen, K. W. Sun, *Sol. Energy Mater. Sol. Cells* **2010**, *94*, 930.  
[24] S. Xu, C. Lao, B. Weintraub, Z. L. Wang, *J. Mater. Res.* **2008**, *23*, 2072.  
[25] S. Xu, N. Adiga, S. Ba, T. Dasgupta, C. F. J. Wu, Z. L. Wang, *ACS Nano* **2009**, *3*, 1803.  
[26] J. Zhu, Z. F. Yu, G. F. Burkhard, C. M. Hsu, S. T. Connor, Y. Q. Xu, Q. Wang, M. McGehee, S. H. Fan, Y. Cui, *Nano Lett.* **2009**, *9*, 279.  
[27] R. Brendel, in *Proc. 12th Eur. Photovoltaic Sol. Energy Conf.* (Eds. R. Hill, W. Palz, P. Helm), H.S. Stephens & Associates, Bedford, UK **1994**, 1339.  
[28] M. Hill, *Handbook of Optics*, 2nd edition, McGraw-Hill, New York **1994**, 2.  
[29] P. L. C. Lolgen, J. A. Eikelboom, R. A. Steeman, W. C. Sinke, L. A. Verhoef, P. F. A. Alkemade, E. Algra, *Proc. 23rd IEEE Photovoltaic Specialists Conf.* (Ed. M. L. Timmons), IEEE, New York **1993**, 236.  
[30] P. A. Basore, *IEEE Trans. Electron Devices* **1990**, *37*, 337.  
[31] Y. Liu, Y. H. Xiu, D. W. Hess, C. P. Wong, *Langmuir* **2010**, *26*, 8908.  
[32] Y. Xiu, L. Zhu, D. W. Hess, C. P. Wong, *Nano Lett.* **2007**, *7*, 3388.  
[33] Z. Y. Lin, Y. Liu, C. P. Wong, *Langmuir* **2010**, *26*, 16110.  
[34] L. L. Cao, H. H. Hu, D. Gao, *Langmuir* **2007**, *23*, 4310.  
[35] J. Zhu, C. M. Hsu, Z. F. Yu, S. H. Fan, Y. Cui, *Nano Lett.* **2010**, *10*, 1979.